Proposal to Jefferson Lab PAC 33

Investigation of the Role of Nuclear Medium Modifications in the ^{4}He$(\vec{e}, e'\vec{p})^3$H Reaction in Hall C

(December 9, 2007)

E. Brash (co-spokesperson)
Christopher Newport University, Newport News, VA

C. Perdrisat
College of William and Mary, Williamsburg, VA

P.E.C. Markowitz
Florida International University, Miami, FL

J.R. Vignote
Gesellschaft für Schwerionenforschung, Darmstadt, Germany

M. Kohl
Hampton University, Hampton, VA

P. Bosted, A. Camsonne, R. Ent, D. Gaskell, D. Higinbotham, T. Horn
Jefferson Lab, Newport News, VA

A. Puckett
Massachusetts Institute of Technology, Cambridge, MA

V. Punjabi, F.R. Wesselmann
Norfolk State University

S. Danagoulian
North Carolina A&T State University, Greensboro, NC

P.M. King
Ohio University, Athens, OH

L.B. Weinstein
Old Dominion University, Norfolk, VA

R. Gilman, R. Ransome (co-spokesperson)
Rutgers University, Piscataway, NJ

A.J. Sarty
Saint Mary's University, Halifax, NS, Canada

J. Glister
Saint Mary's University and Dalhousie University, Halifax, NS, Canada

B. Hu, W. Luo, X. Zhang, Y. Zhang

School of Nuclear Science and Technology, Lanzhou University, Lanzhou, China

B.L. Berman, Y. Ilieva, R. Nasseripour

The George Washington University, Washington, DC

J.M. Udias

Universidad Complutense, Madrid, Spain

G. Rosner

University of Glasgow, Glasgow, United Kingdom

E. Frlez

University of Virginia, Charlottesville, VA

C. Butuceanu, G.M. Huber (co-spokesperson), G.J. Lolos, Z. Papandreou

University of Regina, Regina, SK, Canada

C. Djalali, R. Gothe, K. Park, S. Malace, M. Paolone, S. Strauch (co-spokesperson), D. Tedeschi, M. Wood

University of South Carolina, Columbia, SC

G. Ron, E. Piasetzky, I. Pomerantz, R. Shneor

University of Tel Aviv, Israel

Abstract

Polarization transfer in quasi-elastic nucleon knockout is sensitive to the properties of the nucleon in the nuclear medium, including possible modification of the nucleon form factor and/or spinor. A series of recent experiments at MAMI and Jefferson Lab measured the proton recoil polarization in the $^4\text{He}(\vec{e}, e'\vec{p})^3\text{H}$ reaction for Q^2 between 0.4 and 2.6 $(\text{GeV}/c)^2$. The measured ratios of polarization-transfer coefficients differ from a fully relativistic calculation, favoring either the inclusion of a medium modification of the proton form factors predicted by a quark-meson coupling model, or strong charge-exchange final-state interactions. However, the measured induced polarizations are not consistent with strong charge-exchange final-state interaction model, but agree well with the fully relativistic calculation. This indicates the importance of measuring a broad set of polarization observables, rather than just the polarization-transfer ratio, in order to constrain possible interpretations of the data.

To shed more light on possible proton medium modifications, we propose to measure the polarization-transfer observables P'_x and P'_z and the induced polarization P_y in both the $^4\text{He}(\vec{e}, e'\vec{p})^3\text{H}$ and $^2\text{H}(\vec{e}, e'\vec{p})n$ reactions at Q^2 values of 0.4, 0.7, 1.4, 1.6, 2.2 and 2.4 $(\text{GeV}/c)^2$ in addition to $\vec{e}p$ elastic scattering data. At the two lowest Q^2 settings, we also plan to cover a wide range of missing momenta from -280 to 280 MeV/c to probe different virtualities of the knocked out proton.

1   Physics Motivation

The underlying theory of strong interactions is Quantum ChromoDynamics (QCD), yet there are no ab-initio calculations of nuclei available. Nuclei are effectively and well described as clusters of protons and neutrons held together by a strong, long-range force mediated by meson exchange, whereas the saturation properties of nuclear matter arise from the short-range, repulsive part of the strong interaction [1]. At nuclear densities of about 0.17 nucleons/fm^3, nucleon wave functions have significant overlap. In the chiral limit, one expects nucleons to lose their identity altogether and nuclei to make a transition to a quark-gluon plasma [2]. This phase transition is extensively being studied at the RHIC facility.

Within QCD, there is no known way to derive anything like an atomic nucleus in which the constituents do not change as the mean density (or temperature) goes away from zero [3]. Perhaps the most studied of these effects is the density and temperature dependence of the vector meson masses and widths, which has been treated extensively in a variety of approaches, including chiral symmetry restoration, quark-meson coupling models, and enhanced nuclear isobar interactions [4, 5, 6, 7, 8]. The conclusion that the masses and widths of the nuclear constituents are reduced from their free values is supported by Lattice QCD calculations [9], which suggest that chiral symmetry will be fully restored at $T_c \geq 150$ MeV and/or $\rho_c \geq 5$ ρ_0. Suggestive experimental evidence comes from dilepton production in S+Au and S+W collisions at 200 GeV/u [10], which support a density-dependent ρ^0 mass reduction which is consistent with chiral symmetry restoration as well as with ρ^0-medium rescattering. Other evidence in favor of density dependent mass and width modifications comes from $\omega^0 \to \pi^0\gamma$ photoproduction studies at the Bonn ELSA facility [11], and $p+A$ dilepton production at 12 GeV at KEK [12]. At Jefferson Lab, the CLAS Collaboration studied dilepton photoproduction from titanium and iron, but found only the expected collisional broadening [13]. The structure of the nucleons is also predicted to be modified by the nuclear medium [14], but the experimental situation is even less clear.

The discovery of the nuclear EMC effect almost twenty years ago brought the subjects of quarks into nuclear physics with great impact. However, the specific causes of the modifications observed in the nuclear structure functions have not yet been identified with certainty [15]. Miller and Smith [16] argue that the depletion of the deep inelastic structure function observed in the valence quark regime is due to some interesting effect involving dynamics beyond the conventional nucleon-meson treatment of nuclear physics.

One such explanation is a medium modification of bound nucleon form factors, which also carries implications for the nuclear EMC effect [17]. For example, strong constraints on models of the nuclear EMC effect which assume a large deformation of the intrinsic structure of the nucleon in medium are placed by quark-hadron duality relations between the medium modification of the nucleon form factors and the modification of the deep-inelastic structure function of the bound proton [18]. The acquisition of additional data sensitive to the medium modification of the nucleon form factors would thus advance our understanding of the cause of the EMC effect. The connection between the modifications induced by the nuclear medium of the nucleon form factors and of the deep inelastic structure functions is also discussed by Liuti [19] using the concept of generalized parton distributions.

A variety of models predict measurable deviations from the free space nucleon form factor ratio G_E/G_M in nuclear matter. A calculation by Lu *et al.* [20], using a quark-meson coupling (QMC) model and nuclear density profiles for nuclei from ^{4}He to ^{208}Pb, suggest measurable deviations for all from the free G_E/G_M values of up to 20% over Q^2 range $0.0 < Q^2 < 2.5$ $(\text{GeV}/c)^2$. The ^{4}He nucleus is argued to be the lightest nucleus that can be approximated by a continuous matter distribution. However, because the sampled density is comparable to that of a larger nucleus, the form factor ratio modification in ^{4}He is predicted to be comparable to the modification for the $1s_{1/2}$ shell of ^{16}O. The Lu *et al.* calculation is consistent with present constraints on possible medium modifications for both the electric form factor (from the Coulomb Sum Rule, for $Q^2 < 0.5$ $(\text{GeV}/c)^2$ [21, 22, 23]) and the magnetic form factor (from a y-scaling analysis [24] for $Q^2 > 1$ $(\text{GeV}/c)^2$), and limits on the scaling of nucleon magnetic moments in nuclei [25].

Similar measurable deviations from the free space G_E/G_M ratio have been calculated in the light-front constituent quark model of Frank *et al.* [26]. Yakshiev *et al.* [27] investigated possible modifications to the nucleons' electromagnetic form factors in the ^{4}He nucleus in the framework of a modified Skyrme model, but only for $Q^2 < 0.6$ $(\text{GeV}/c)^2$. The modification effects are calculated to be small but increase steadily with Q^2, and are dependent upon the distance of the nucleon from the dense core at the center of the nucleus. Smith and Miller studied the electromagnetic form factors of a bound proton in the framework of a chiral quark-soliton (CQS) model for the proton [28]. They found that the ratio of the isoscalar electric to the isovector magnetic form factor decreases by 20% at $Q^2 = 1$ $(\text{GeV}/c)^2$ at nuclear density, but they do not see a strong enhancement of the magnetic moment; see Fig. 1 for a comparison of the QMC- and CQS-model results. Thus, although models using free nucleons and mesons as quasi-particles are successful in the description of many aspects of nuclear physics, one may expect that, under certain circumstances, their use is a highly uneconomical approach, especially given that these are not the fundamental entities of the underlying theory. The use of medium-modified nucleons as quasi-particles may be a better choice.

To experimentally demonstrate any modification of the nucleon form factors, one is required to have excellent control over the reaction mechanism effects [29]. The nucleus, as a bound many-body quantum system, has inherent many-body effects, such as meson-exchange currents (MEC) and isobar configurations (IC). In addition, when probing nuclear structure one has to deal with final-state interactions (FSI). A change in the spatial structure of the nucleon, as expressed in medium modifications of the nucleon form factors, implies that one treats observed medium effects as density dependent one-body effects, and assumes that the major part of the many-body effects are therein incorporated. If medium-modified nucleon form factors are defined, in principle medium-modified many body effects are also required in order to perform a rigorous calculation of nuclear structure.

There is no experimental way to distinguish between both approaches: the notion of medium modification of single particle properties like, *e.g.*, the electromagnetic form factors of a nucleon, in a nuclear environment is a purely theoretical concept [30]. Thus, distinguishing possible changes in the spatial structure of nucleons embedded in a nucleus from more conventional many-body effects is only possible within the context of a
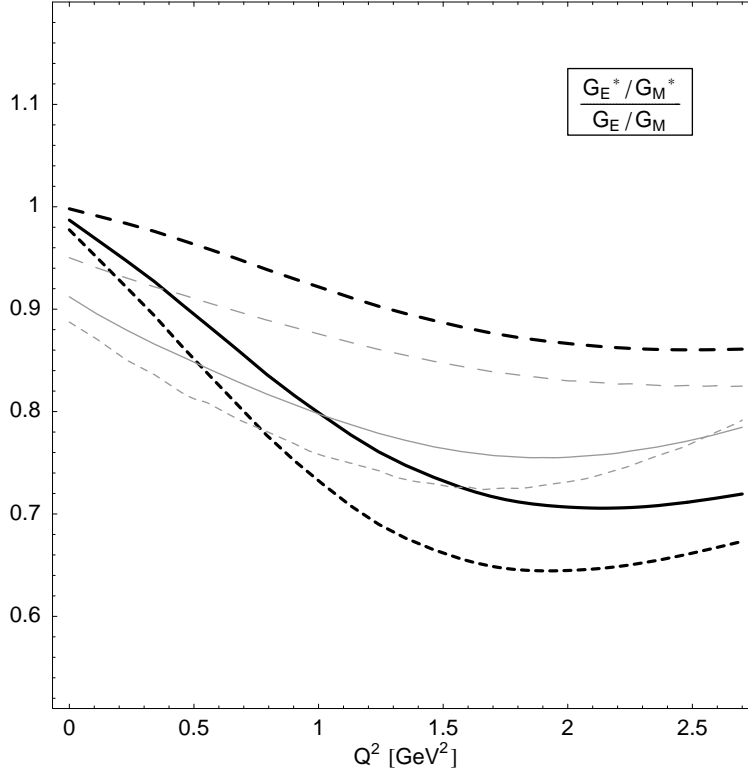
Figure 1: The double ratio, $(G_E(Q^2)/G_M(Q^2))_{\mathrm{medium}}/(G_E(Q^2)/G_M(Q^2))_{\mathrm{free}}$, of the electric to magnetic form factors in nuclear matter and in the vacuum from the CQS model [28] (heavy) and the QMC model [20] (light). Three densities are shown: $0.5\rho_0$ (long dashes), $1.0\rho_0$ (solid), and $1.5\rho_0$ (short dashes). Figure taken from [28].

model. We argue the quasi-elastic proton knockout in the proposed $^4\mathrm{He}(\vec{e}, e'\vec{p})\,^3\mathrm{H}$ reaction to be the most directly accessible experimental method to challenge conventional meson-nucleon modelling where these conventional effects are suppressed.

2 Recoil Polarization in Quasi-Elastic Electron Scattering

2.1 Polarization Transfer

In unpolarized $\mathrm{A}(e, e'p)$ experiments involving light- and medium-mass nuclei, deviations were observed in the longitudinal/transverse character of the nuclear response compared to the free proton case [31, 32, 33]. Below the two-nucleon emission threshold, these deviations were originally interpreted as changes in the nucleon form factors within the nuclear medium. However, strong interaction effects on the ejected proton (final state interactions [FSI]) later also succeeded in explaining the observed effect [34]. This illustrates that any interpretation in terms of medium modifications to nucleon form factors requires having excellent control of FSI effects. Tantalizing hints of medium effects were observed for unpolarized longitudinal/transverse separations in the $^4\mathrm{He}(e,e'p)^3\mathrm{H}$ reaction [35, 36]. The apparent reduction of the in-medium G_{E_p} implied by impulse-approximation interpretation of the L/T-ratios measured in $^4\mathrm{He}$ is, however, not confirmed in a recent calculation by Carlson *et al.* [37].

Polarization transfer in quasi-elastic nucleon knockout is sensitive to the properties of the nucleon in the

nuclear medium, including possible modification of the nucleon form factor and/or spinor. This can be seen from free electron-nucleon scattering, where the ratio of the electric to magnetic Sachs form factors, G_E and G_M, is given by [38]:

$$\frac{G_E}{G_M} = -\frac{P'_x}{P'_z} \cdot \frac{E_e + E_{e'}}{2m_p} \tan(\theta_e/2), \tag{1}$$

where P'_x and P'_z are the transverse and longitudinal transferred polarizations; see Fig. 2. The beam energy is E_e, the energy (angle) of the scattered electron is $E_{e'}$ (θ_e) and m_p is the proton mass.
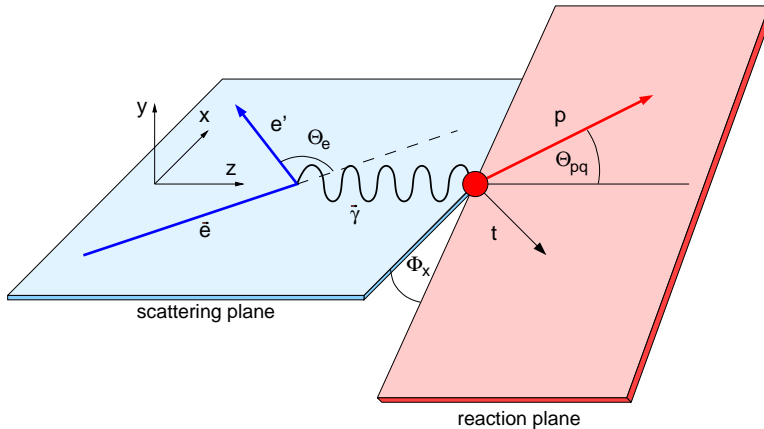

Figure 2: Coordinate system used to define the components of the recoil proton polarization in the $^4\mathrm{He}(\vec{e}, e'\vec{p})\,^3\mathrm{H}$ reaction. The z axis is along the momentum transfer, the x axis is in the scattering plane perpendicular to the momentum transfer $\vec{q}$ and the y axis is perpendicular to the scattering plane, forming a right-handed system.

This relation was recently used to extract G_E/G_M for the proton, see *e.g.* [39, 40, 41, 42]. For quasi-elastic nucleon knockout of a bound proton, this relation is only approximately correct, but polarization transfer remains sensitive to the properties of the nucleon in the nuclear medium. A proper interpretation of the results requires accounting for such effects as FSI and MEC. At high momentum transfer, however, the contribution of many-body and rescattering mechanisms are strongly suppressed and spin observables provide us with a way to study the behavior of the nucleon form factors in the nuclear medium [43].

2.2   Previous Experimental Results

Polarization transfer has been used previously to study nuclear medium effects in deuterium [44, 45, 46]. Within statistical uncertainties, no evidence of medium modifications was found. More recently, polarization-transfer data on $^2\mathrm{H}$ were measured in JLab experiment E89-028 [47], under conditions very similar to those for experiment E93-049 on $^4\mathrm{He}$. Realistic calculations to describe this reaction were performed by Arenhövel [48]. Experimental results (open triangles) for the $^2\mathrm{H}$-to-$^1\mathrm{H}$ polarization-transfer double ratio, along with the results of a calculation by Arenhövel (dashed curve), are shown in Fig. 3. The results are expressed in terms of the polarization double ratio

$$R = \frac{(P'_x/P'_z)_{^2\mathrm{H}}}{(P'_x/P'_z)_{^1\mathrm{H}}}. \tag{2}$$

Here, the deuterium polarization ratio is normalized to the hydrogen polarization ratio measured in the identical setting. Such a double ratio cancels nearly all experimental systematic uncertainties. The calculation includes final-state interactions (FSI), meson-exchange currents (MEC), and isobar configurations (IC), as
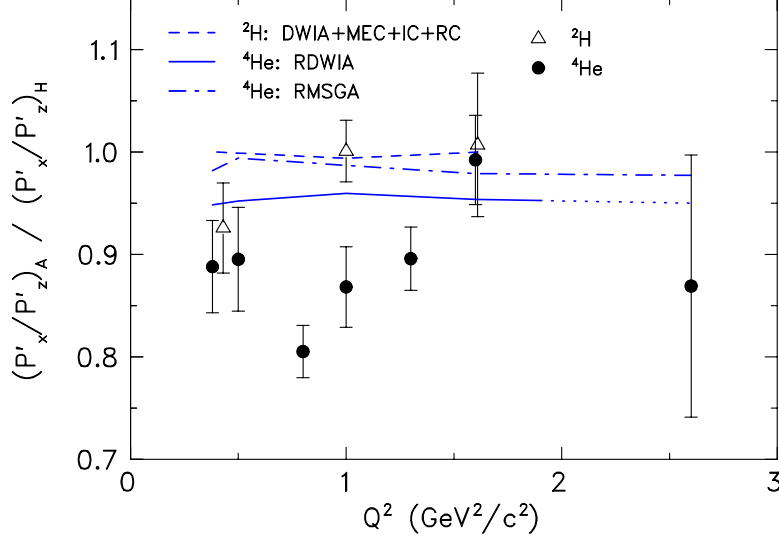
Figure 3: Bound-to-free polarization-transfer double ratio R for $^2\mathrm{H}(\vec{e}, e'\vec{p})n$ (open triangles) from [47] and for $^4\mathrm{He}(\vec{e}, e'\vec{p})^3\mathrm{H}$ (closed circles) from [50, 51, 52] as a function of Q^2. The curves show results of a calculation by Arenhövel (dashed line) for deuterium, a RDWIA calculation for helium by Udias *et al.* (solid line) [53], and a relativistic Glauber model calculation for helium by Lava *et al.* (dash-dotted line) [54]. While the deuterium data are consistent with the conventional model, the helium data are not. The helium data from E03-104 at 0.7 and 1.3 $(\mathrm{GeV}/c)^2$ are still preliminary and their final uncertainties are expected to be smaller.

well as relativistic contributions (RC) of leading order in p/m to the kinematic wave function boost and to the nucleon current. Arenhövel's full calculation describes the $^2\mathrm{H}$ data well. As the sampled density is small, it is not surprising that there are no indications for medium modifications of the proton electromagnetic form factors in the $^2\mathrm{H}$ data.

One might expect to find larger medium effects in $^4\mathrm{He}$, with its significantly higher density. Indeed, recent Jefferson Lab Experiment E03-103 has measured the EMC effect for various nuclei and preliminary results indicate that the nuclear dependence of the cross section is nearly identical for $^4\mathrm{He}$ and $^{12}\mathrm{C}$ [49]. Although estimates of the many-body effects in $^4\mathrm{He}$ may be more difficult than in $^2\mathrm{H}$, calculations for $^4\mathrm{He}$ indicate they are small [43]. The first $^4\mathrm{He}(\vec{e}, e'\vec{p})^3\mathrm{H}$ polarization-transfer measurements were performed at the Mainz microtron (MAMI) at $Q^2 = 0.4$ $(\mathrm{GeV}/c)^2$ [50] and at Jefferson Lab Hall A at $Q^2 = 0.5, 1.0, 1.6$, and 2.6 $(\mathrm{GeV}/c)^2$, E93-049 [51]. Our recent experiment E03-104 [52] extended these measurements with two high-precision points at $Q^2 = 0.8$ and 1.3 $(\mathrm{GeV}/c)^2$. All these data were taken in quasi-elastic kinematics at low missing momentum with symmetry about the three-momentum-transfer direction to minimize conventional many-body effects in the reaction. The results are shown in Fig. 3 (solid points). In each experiment, two high-resolution spectrometers were used to detect the scattered electron and the recoiling proton. The missing-mass technique was used to identify $^3\mathrm{H}$ in the final state. As these experiments were designed to detect differences between the in-medium polarizations compared to the free values, both $^4\mathrm{He}$ and $^1\mathrm{H}$ targets were used (due to beam-time constraints, only $^4\mathrm{He}$ data were acquired at $Q^2 = 2.6$ $(\mathrm{GeV}/c)^2$). The systematic uncertainty, predominantly due to uncertainties in the spin transport through the magnetic fields of the spectrometer, is estimated to be 1.3% at $Q^2 = 1.0$ $(\mathrm{GeV}/c)^2$. The polarization-transfer ratio (P'_x/P'_z) in the $(\vec{e}, e'\vec{p})$ reaction on helium is significantly different from those on deuterium or hydrogen.

In Fig. 3, the helium data are compared with result of a relativistic distorted-wave impulse approximation (RDWIA) calculation by the Madrid group [55, 53] (solid curve). The calculation gives an R value slightly smaller than one (by $\approx 3\%$) but overpredicts most of the experimental data. We note that these relativistic calculations provide good descriptions of, e.g., the induced polarizations as measured at Bates in the ^{12}C$(e,e'\vec{p})$ reaction [56] and of A_{TL} in ^{16}O$(e,e'p)$ as previously measured at JLab [57]. The calculation shown uses the Coulomb gauge, the $cc1$ current operator as defined in [58], and the MRW optical potential of [59]. The $cc2$ current operator gives higher values of R, worsening agreement with the data. In general, various choices for, e.g., spinor distortions, current operators, and relativistic corrections affect the theoretical predictions by $\leq 3\%$ within the RDWIA model, and presently can not explain the disagreement with the data and the RDWIA calculation. The data are also compared with results from a relativistic Glauber model by the Ghent group [54], which gives $R/R_{\rm PWIA}$ of about one.

2.3 Interpretation of the Polarization Transfer Data

As shown in Fig. 3, the RDWIA calculation overpredicts the mean trend of the data by about 6%. After including in the RDWIA calculation the density dependent medium-modified form factors of Lu *et al.* [20] (solid curve in the left panel of Fig. 4), good agreement with the data is obtained. The model results have been carefully integrated over the experimental acceptance of the data in order to make the comparison as meaningful as possible. We do not show a chiral-soliton model calculation of the in-medium form factors by Smith and Miller [28], which give results similar to the QMC results. This agreement has been interpreted as a
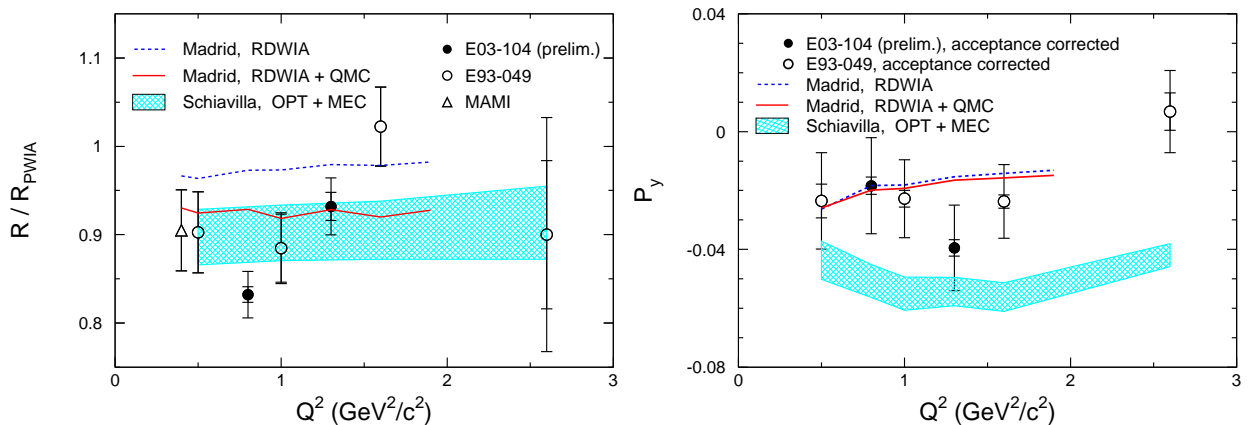

Figure 4: ^{4}He$(\vec{e},e'\vec{p})^3$H data as a function of Q^2 from Mainz [50] and Jefferson Lab experiment E93-049 (open symbols) [51] along with preliminary results from experiment E03-104 (filled circles), compared to calculations from the Madrid group [55] and Schiavilla *et al.* [60]. [**Left:**] Superratio $R/R_{\rm PWIA}$, where R is the ratio of transverse to longitudinal polarization of the recoiling proton in ^{4}He$(\vec{e},e'\vec{p})^3$H compared to the same ratio for ^{1}H$(\vec{e},e'\vec{p})$. The baseline $R_{\rm PWIA}$ is the value of R obtained in a plane-wave calculation, to account for the 'trivial' effects of free *vs.* moving proton. [**Right:**] Induced polarization P_y for missing momentum $p_m \approx 0$; note that the experimental data have been corrected for the spectrometer acceptance.

possible evidence of proton medium modifications [51]. The observed suppression of the polarization-transfer ratio has been equally well described in a more traditional calculation by Schiavilla *et al.* [60] using free form factors by including charge-exchange final-state interactions and two-body charge and current operators (shaded band). Yet, the choice of the parameters for the charge-exchange FSI is not well constrained by

data.

The difference in the modeling of final-state interactions by the various groups is the origin of the major part of the difference between the results of Udias *et al.* [55] and of Schiavilla *et al.* [60] for the polarization observables. Effects from final-state interactions can be studied experimentally with the induced polarization, P_y. These induced polarizations are identically zero in the absence of FSI effects (in the one-photon exchange approximation) and constitute a stringent test of the various model calculations. The right panel of Fig. 4 shows the data for P_y. The induced polarization is small in this reaction. The sizable systematic uncertainties are due to possible instrumental asymmetries. Dedicated data have been taken during E03-104 to study these and we hope to significantly reduce the systematic uncertainties in P_y in the final analysis. The data are compared with the results of the calculations from the Madrid group and Schiavilla *et al.* at missing momenta of about zero. The data have been corrected for the spectrometer acceptance to facilitate this comparison. For the induced polarization, the RDWIA curves with (solid) and without (dotted) medium modifications are almost identical. Presently, the data seem to indicate good agreement with the RDWIA calculation of Udias *et al.* [55, 53] and suggest that the magnitude of the induced polarization (and thus particularly the charge-exchange final-state interaction) is overestimated in the model of Schiavilla *et al.* [60]. This may also impact the superratio prediction by this model.

The sensitivity of recoil polarization observables in $A(\vec{e}, e'\vec{p})B$ reactions to channel coupling in final-state interactions was also investigated by Kelly [61]. Calculations were performed for ^{12}C and ^{16}O. In these studies, it was found that polarization transfer observables for proton knockout with modest missing momentum appear to be quite insensitive to details of the final-state interaction, including channel coupling. We estimate the effect of channel coupling for the ^{4}He$(\vec{e}, e'\vec{p})^3$H reaction by calculating the relative difference between the polarization transfer ratio with (R_{CC}), and without channel coupling (R). Couplings between the proton $1s_{1/2}$ and neutron $1s_{1/2}$ states were considered. The calculation followed the approach of Kelly [61] and found a minimal effect, on average of the order of $1\% - 2\%$ for $|p_m| < 100$ MeV/c.

A comparison of the model calculations in the left and right panels of Fig. 4 shows that the in-medium form factors (solid curves) mostly affect the ratio of polarization-transfer observables, not the induced polarization. It is a key element of the recoil polarization experiments, as the one proposed here, to have access to both of these observables.

3   The Proposed Experiment

In this experiment, we propose to take production data on three targets: ^{1}H, ^{2}H, and ^{4}He. The data on hydrogen will provide the reference point for elastic electron scattering on a free proton. As the induced polarization P_y from hydrogen is zero in the one-photon-exchange approximation, these data will also help to understand the instrumental asymmetries of the Focal Plane Polarimeter (FPP).

The data on deuterium will provide a link between free ep scattering and quasi-elastic proton knockout in ^{4}He. The ^{2}H and ^{4}He data have in common that in both cases the reaction takes place on a bound, off-shell nucleus and a comparison of missing-momentum distributions are possible. The proton in helium, however, is tightly bound in a nuclear medium which is much denser than that in deuterium and medium effect will become apparent in a comparison between both of these data.

The target nucleus ^{4}He is optimal for further study since its relative simplicity allows for realistic microscopic calculations and since its high density enhances any possible medium effects. Also, a variety of calculations for the ^{4}He$(\vec{e}, e'\vec{p})^3$H reaction indicate that polarization transfer observables are influenced little by FSI and MEC effects, amounting to only about a 10% correction [43, 55, 62]. It is precisely these effects (especially FSI) that have so far prevented a clean determination of nucleon medium modifications from

unpolarized response functions in $(e, e'p)$ experiments. If, instead of ^{4}He, one would be able to use a heavier target nucleus, or any nuclear transition, that effectively probes some higher nuclear density region than in the $^4\mathrm{He}(\vec{e}, e'\vec{p})\,^3\mathrm{H}$ reaction, this would be worthwhile. However, in terms of the effective density sampled in the $(e, e'p)$ reaction, ^{4}He is only marginally less dense than heavier nuclei. The average density as sampled in, e.g., the $^{16}\mathrm{O}(e, e'p)$ reaction is only slightly larger than that for the $^4\mathrm{He}(e, e'p)$ reaction (which is about 0.25 times the nuclear matter density), whereas microscopic calculations may be more troublesome, and experimental rates are smaller. Furthermore, Coulomb corrections are more of an issue for heavier nuclei. On the technical side, ^{4}He can easily withstand high beam currents (possible target boiling effects do not affect the polarization measured). Therefore, ^{4}He remains the target of choice.

The preliminary results from E03-104 possibly hint at an unexpected trend in the Q^2 dependence of R. This is particularly interesting, as different calculations of in-medium form factors yield widely differing Q^2-dependence predictions. For example, the Nambu-Jona-Lasinio model of Horikawa and Bentz [63], predicts a decrease of medium modifications with increasing Q^2. The authors argue that this is consistent with the intuitive expectation that the mean fields, which reflect the long-range nuclear correlations, should not influence the structure of the nucleon at short distances. Their predicted decrease in nuclear medium modifications with Q^2 is in dramatic contrast to the increase in modifications with Q^2 predicted by the QMC and CQS models shown in Fig. 1. We propose to improve on the precision of the polarization double ratios and induced polarizations over a wide range of Q^2, with six new data points from 0.40 $(\mathrm{GeV}/c)^2$ up to 2.42 $(\mathrm{GeV}/c)^2$; see Fig. 5. The proposed data are integrated over a missing momentum range of $|p_m| < 100$ MeV/c for $Q^2 = 0.4$, 0.7 $(\mathrm{GeV}/c)^2$, and $|p_m| < 175$ MeV/c for $Q^2 > 1.2$ $(\mathrm{GeV}/c)^2$.
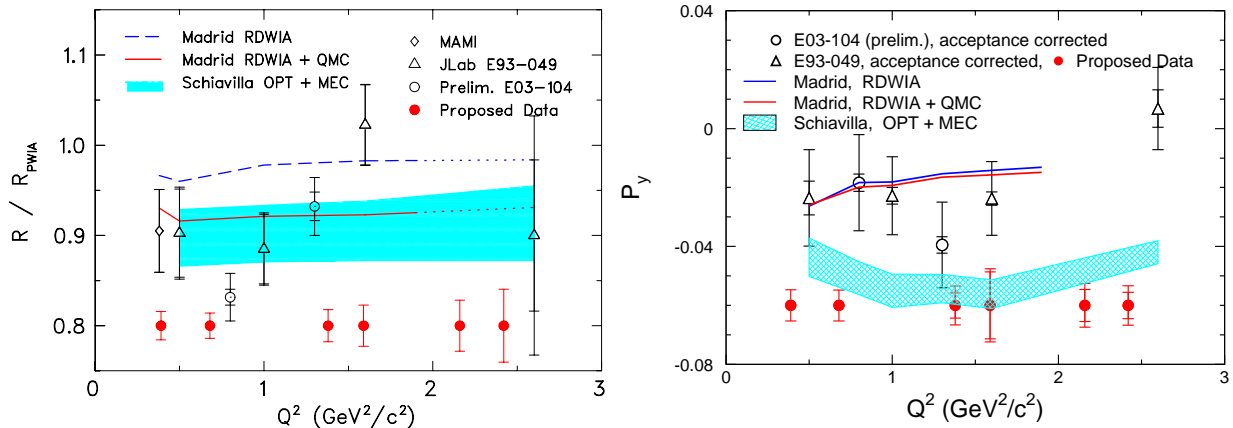

Figure 5: Previous polarization-transfer double ratios (left) and induced polarization data (right) for $^4\mathrm{He}(\vec{e}, e'\vec{p})\,^3\mathrm{H}$ (open symbols) along with total uncertainties of the proposed data (solid points). The data are compared with various model calculations; as in for Fig. 4. For the P_y data points, the inner bar reflects statistical uncertainties only, while the outer bar includes the effect of projected experimental systematic uncertainties.

Ciofi *et al* [64] argue that the modification of the wave function of the bound nucleon in a nucleus should strongly depend on the momentum of the nucleon. We are therefore proposing to study the polarization-transfer ratio not only at small values of missing momentum, where reaction-mechanism effects were shown to be small, but also at larger values of missing momentum, in order to test this argument. These expected data could put much stronger constraints on possible medium effects, including the medium-modification of
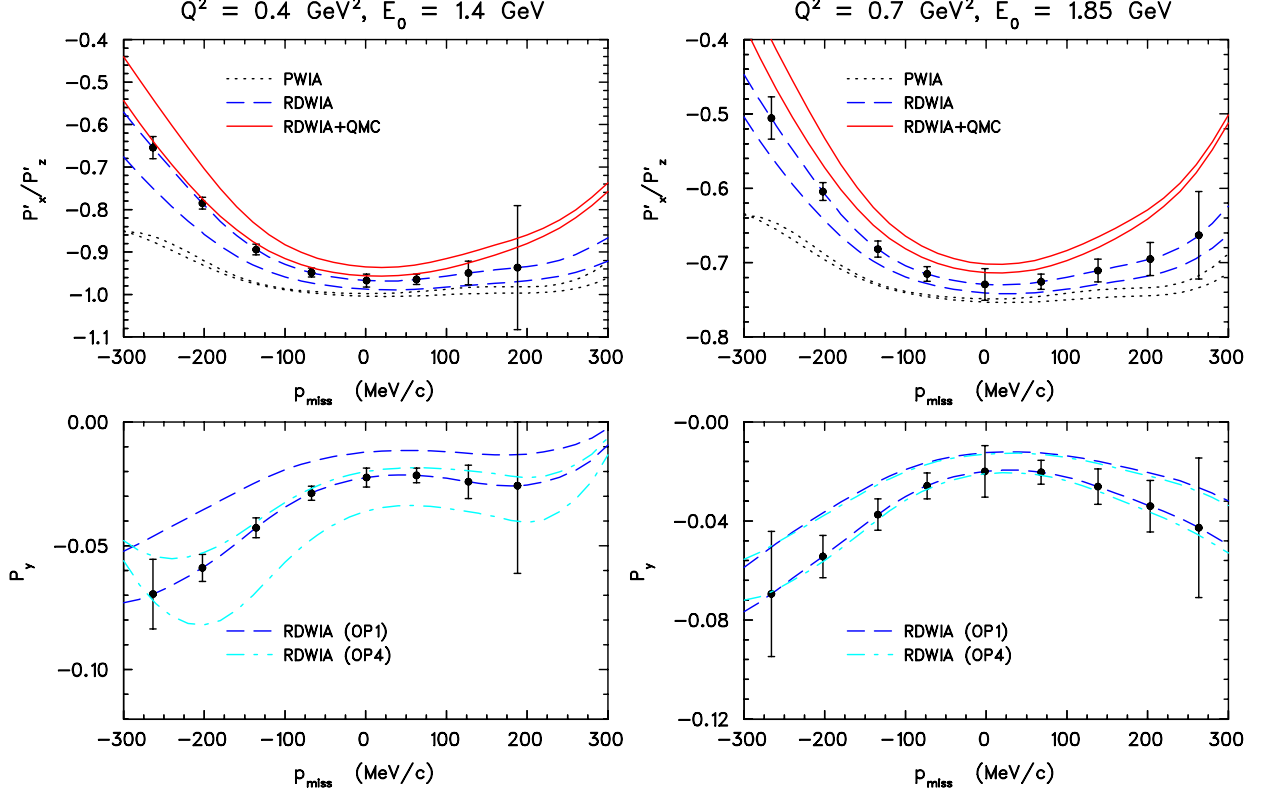
Figure 6: Polarization-transfer ratio (upper panels) and induced polarization (lower panels) in the $^4\text{He}(\vec{e}, e'\vec{p})^3\text{H}$ reaction at $Q^2 = 0.4$ (GeV/c)^2 and $Q^2 = 0.7$ (GeV/c)^2 in parallel kinematics. The curves are various calculations using the model of Udias *et al.* for the current operators $cc1$ and $cc2$; OP1 and OP4 refer to different choices in the optical potential. While the ratio is relatively insensitive to the choice of optical potential, P_y is more sensitive. The points indicate the statistical uncertainties of the proposed data and are placed on the RDWIA-$cc1$ curves.

the proton structure, than the previous data do. The missing-momentum coverage and precision of these data are shown in Fig. 6 for the $Q^2 = 0.4$ (GeV/c)^2 and $Q^2 = 0.7$ (GeV/c)^2 settings, respectively. For the higher Q^2 settings, the missing momentum coverage will be limited to $|p_m| < 175$ MeV/c.

Summary

Polarization transfer in quasi-elastic proton knockout in the $^4\text{He}(\vec{e}, e'\vec{p})^3\text{H}$ reaction is arguably one of the most direct experimental methods to identify nuclear-medium changes to nucleon properties, which are predicted by QCD-based models, as other conventional medium effects, such as many-body currents and final state interactions, are suppressed. Furthermore, the possible role of FSI in the interpretation of these data can be constrained by our data on the induced polarization P_y.

In continuation of the series of our earlier experiments at MAMI and JLab Hall A (E93-049 and E03-104), we propose to measure the proton-recoil polarization observables P'_x, P'_z, and P_y in the $^4\text{He}(\vec{e}, e'\vec{p})^3\text{H}$ reaction in Hall C. Key features of the new experiment include:

1. The preliminary $^4\text{He}(\vec{e}, e'\vec{p})^3\text{H}$ results from E03-104 suggest a changing polarization-transfer superratio

with Q^2 — in disagreement with all previous model calculations. We propose to improve on the precision of the polarization double ratios and induced polarizations over a wide range of Q^2, with six new data points at $Q^2 = 0.4$, 0.7, 1.4, 1.6, 2.2, and 2.4 $(\text{GeV}/c)^2$ to study thoroughly the Q^2 dependence of possible modifications of in-medium proton form factors.

2. Medium effects are expected to depend strongly on the momentum of the bound nucleon. We propose a significantly improved missing momentum coverage at $Q^2 = 0.4$ and 0.7 $(\text{GeV}/c)^2$. Here, we propose to measure a range almost covering ± 300 MeV/c in parallel kinematics.

3. We propose to take data from $^4\text{He}(\vec{e}, e'\vec{p})\,^3\text{H}$ and $^2\text{H}(\vec{e}, e'\vec{p})n$ to compare knockout data of tightly and weakly bound protons and help in the interpretation of the ^4He data.

4 Proposed Kinematics and Run-Time Estimates

^{4}**He Q^2 Distribution**   As discussed in Section 3, we propose to improve on the precision of the polarization double ratios R over a wide range of Q^2, from 0.40 $(\text{GeV}/c)^2$ up to 2.42 $(\text{GeV}/c)^2$. This can be efficiently accomplished via four settings of the HMS+SOS spectrometers in Hall C since their coincidence acceptance is quite large. The proposed settings are listed in Table 1, all of which are for the proton detection along the q-vector (parallel kinematics). The beam energies listed are optimal in that they allow the best statistical precision per unit time. However, the precision maximum is broad and we can accept other (primarily lower) beam energies in order to be compatible with the requirements of other halls at the time of scheduling.

The coincidence acceptance for our proposed $Q^2 = 1.50$ $(\text{GeV}/c)^2$ setting is shown in Fig. 7. We intend to divide these data into two Q^2 bins, $1.25 < Q^2 < 1.50$ $(\text{GeV}/c)^2$, and $1.50 < Q^2 < 1.75$ $(\text{GeV}/c)^2$, yielding ratio measurements at mean Q^2 values of 1.38 and 1.59 $(\text{GeV}/c)^2$. Similarly, the $Q^2 = 2.30$ $(\text{GeV}/c)^2$ setting can be divided into bins of $2.00 < Q^2 < 2.30$ $(\text{GeV}/c)^2$, and $2.30 < Q^2 < 2.60$ $(\text{GeV}/c)^2$, yielding ratio measurements at mean Q^2 values of 2.16 and 2.42 $(\text{GeV}/c)^2$. Since the absolute momentum acceptances for the lower $Q^2 = 0.40$ and 0.70 $(\text{GeV}/c)^2$ settings are smaller, those data would not be divided in this manner. Missing momentum cuts ($|p_m| < 100$ MeV/c at $Q^2 = 0.4, 0.7$ $(\text{GeV}/c)^2$ and $|p_m| < 175$ MeV/c at all higher Q^2) would be placed to ensure that the missing momentum for each point in the ratio scan averages to near zero. In this manner, ratio measurements at six values of Q^2 can be obtained. These points, as well as their projected ratio uncertainties, are indicated in Fig. 5.

^{4}**He Missing Momentum Studies**   We propose to take additional ^{4}He data at $Q^2 = 0.40$ and 0.70 $(\text{GeV}/c)^2$ spanning a wide range of missing momentum. The justification of these studies is to probe for momentum dependent effects upon the wave function of the bound nucleon. At these lower Q^2, the data come in relatively quickly. Several SOS+HMS coincidence settings are required, where both the energy and momentum transfer are adjusted to ensure that Q^2 and p_m are fixed at the required values. These p_m settings are indicated in the third column of Table 1. The proposed $Q^2 = 0.70$ $(\text{GeV}/c)^2$ coincidence coverage from the five overlapping SOS+HMS coincidence settings is shown in Fig. 8. This provides a missing momentum scan from -266 to $+263$ MeV/c. The missing momentum coverage at $Q^2 = 0.40$ $(\text{GeV}/c)^2$ is similar, except that the highest p_m setting is precluded by the very low proton momentum that would result. The missing momentum coverage for the higher $Q^2 > 1.2$ (GeV/c) settings is limited by the coincidence acceptance coverage of a single HMS+SOS setting, to $|p_m| < 175$ MeV/c, as indicated in Fig. 7.

$^1H(e, e'p)$ **Scans**   We propose to acquire scans of hydrogen elastic scattering events at each of $Q^2 = 0.40$, 0.70 and 1.50 $(\text{GeV}/c)^2$. As shown in Fig. 9, eight settings of HMS momentum, from $\delta_{\text{HMS}} = -14.5\%$ to

Table 1: Proposed parallel kinematics. However, we expect the beam energies ultimately used to differ from these, according to scheduling requirements. The scattered electron will be detected in the SOS and the proton spin analyzed in the HMS FPP. For each Q^2, eight hydrogen elastics settings are planned, spanning the range of HMS momentum indicated.

Q^2 (GeV^2/c^2)	E_e (GeV)	p_m (GeV/c)	$E_{e'}$ (GeV)	$\theta_{e'}$ (deg)	p_p (GeV/c)	θ_p (deg)	Time (Hours)	Current (μA)
^{4}He$(\vec{e}, e'\vec{p})^3$H Settings								
0.400	1.400	+0.125	1.240	27.78	0.527	62.33	18	25
		0.0	1.163	28.70	0.675	55.77	7	35
		-0.125	1.052	30.20	0.847	47.19	7	70
		-0.225	0.929	32.20	1.014	38.86	14	100
0.700	1.850	+0.250	1.637	27.82	0.613	62.23	55	70
		+0.125	1.558	28.53	0.761	57.11	12	100
		0.0	1.450	29.60	0.928	50.54	5	100
		-0.125	1.301	31.29	1.126	42.45	11	100
		-0.225	1.137	33.53	1.324	34.85	34	100
1.500	2.500	0.0	1.664	34.94	1.483	40.01	83	100
2.300	3.000	0.0	1.729	38.89	1.979	33.28	225	100
^{2}H$(\vec{e}, e'\vec{p})n$ Settings								
0.400	1.400	0.0	1.184	28.44	0.668	57.53	1.5	15
0.700	1.850	0.0	1.474	29.35	0.917	51.95	1.5	40
1.500	2.500	0.0	1.697	34.60	1.465	41.12	12	100
2.300	3.000	0.0	1.740	38.43	1.953	34.27	38	100
^{1}H$(e, e'p)$ Scans								
0.400	1.400	0.0	1.187	28.40	0.570–0.747	57.76	8×0.7	4.5
0.700	1.850	0.0	1.477	29.32	0.783–1.026	52.14	8×0.85	15
1.500	2.500	0.0	1.701	34.55	1.251–1.639	41.26	8×2.0	100

^{4}He$(e,e'p)^3$H Q^2=1.50 GeV^2 E=2.50 GeV HMS+SOS

Q2 vs PMsigned t+p Cut
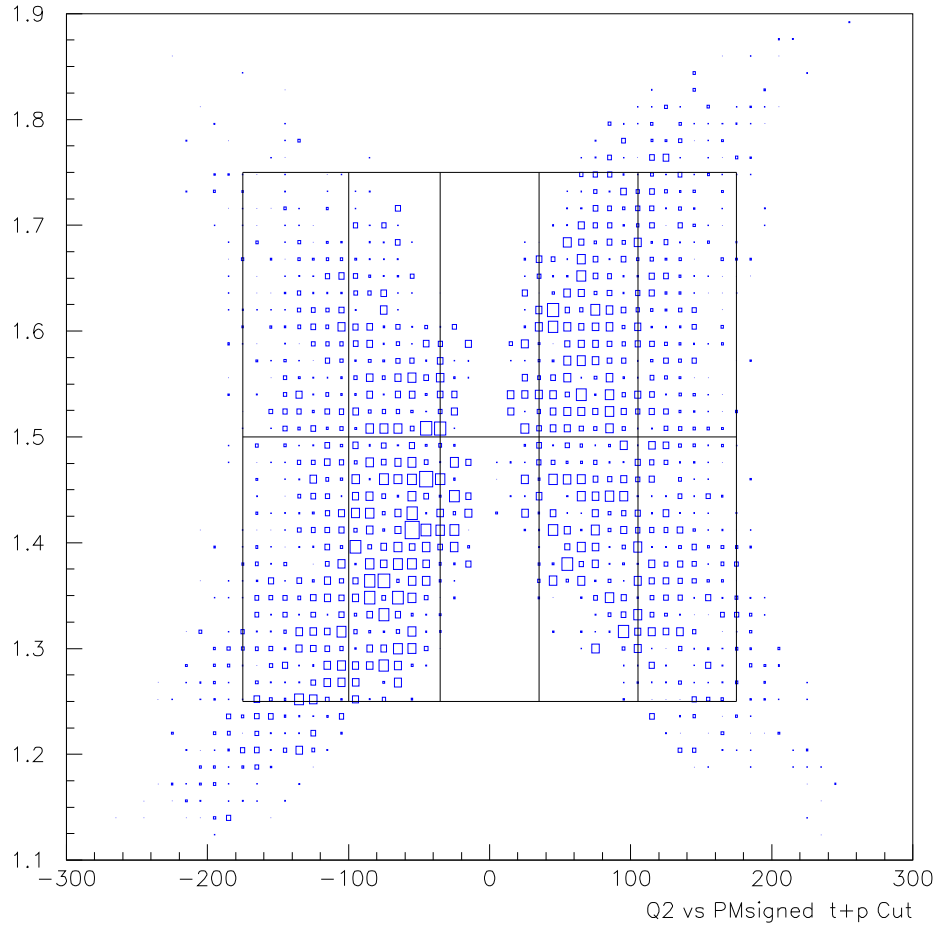
Figure 7: Simulated ^{4}He$(e, e'p)^3$H coverage in Q^2 (y-axis) and missing momentum (x-axis) for the $Q^2 = 1.50$ (GeV/$c)^2$ setting listed in Table 1. The solid lines indicate a possible binning of these data.

Figure 8: Simulated $^4\mathrm{He}(e, e'p)^3\mathrm{H}$ coverage in Q^2 (y-axis) and missing momentum (x-axis) for the $Q^2 = 0.70$ $(\mathrm{GeV}/c)^2$ settings listed in Table 1. The data are color coded according to the central missing momentum value of each setting: $p_m = 0$ (blue), $p_m = 125$ MeV/c (green), $p_m = -125$ MeV/c (red), $p_m = 250$ MeV/c (cyan), and $p_m = -225$ MeV/c (violet). The solid lines indicate a possible binning of these data.

15

1He(e,e´p) Elastics Scan   Q^2=0.40 GeV^2 E=1.40 GeV HMS+SOS

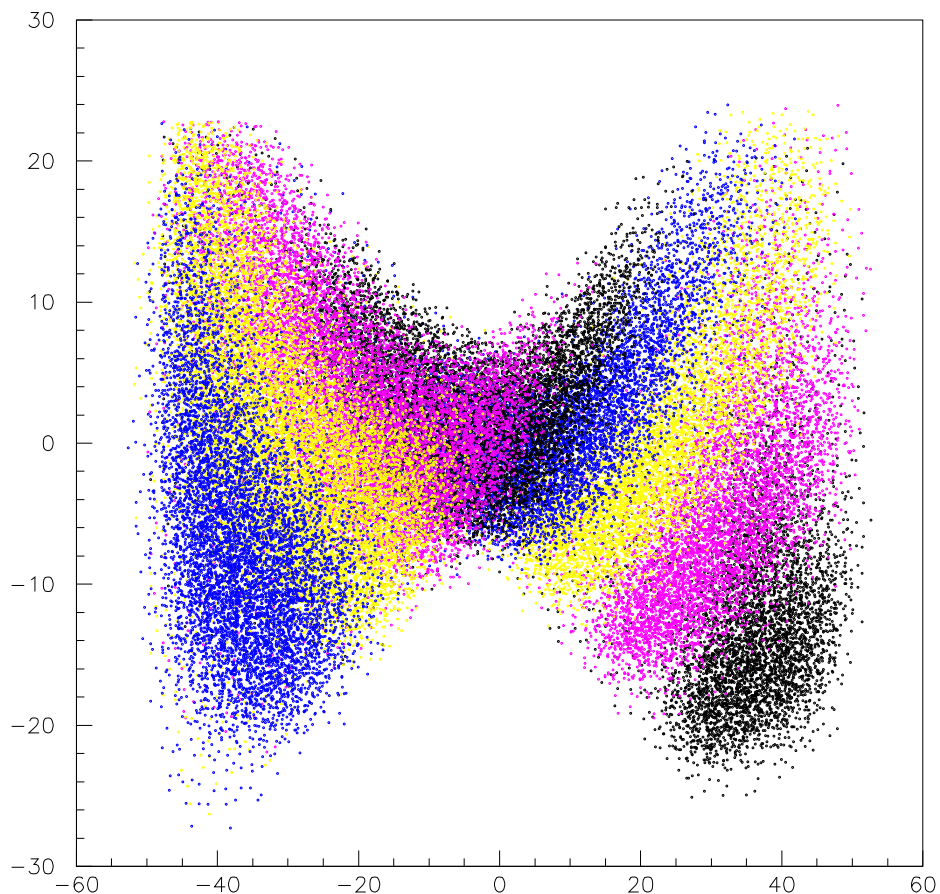Figure 9: Simulated ^{1}H$(e, e'p)$ focal plane scan for the $Q^2 = 0.40$ (GeV/c)^2 settings listed in Table 1. The data are color coded according to the HMS momentum setting. Eight settings, from $\delta_{\mathrm{HMS}} = -14.5\%$ to $+12\%$ will provide good coverage across the HMS focal plane.

$+12\%$ will provide good coverage across the HMS focal plane. This will allow the instrumental asymmetries of the FPP to be studied, as well as to provide a reference for the polarization-ratio measurements. We believe that we will not need to acquire ^{1}H elastic scattering data for our $Q^2 = 2.30$ (GeV/c)^2 setting. The elastic scattering polarization transfer observables are in the process of being measured in Hall C at $Q^2 = 2.47$ (GeV/c)^2 to an uncertainty of $\sim 1\%$ in the "Two Photon Exchange" experiment E04-019 [65]. These data are more than sufficiently precise for our needs, even after including the anticipated extrapolation uncertainty from $Q^2 = 2.47$ (GeV/c)^2 to the $Q^2 = 2.16$ and 2.42 (GeV/c)^2 of our higher Q^2 data.

^{2}**H**$(\vec{e}, e'\vec{p})n$ **Data**   We also propose to take data with a deuterium target at all four Q^2 in order to form a second reference ratio $R = \frac{(P'_x/P'_z)_{4_{He}}}{(P'_x/P'_z)_{2_H}}$. The required settings are listed in Table 1. Our simulations indicate that the deuterium coincidence rate (for same unit luminosity, and after cuts) is a factor of 7 to 15 higher than for ^{4}He, with the ratio dropping as Q^2 increases.

4.1 Instrumentation

Spectrometers This experiment requires a maximum HMS momentum of 2.0 GeV/c, which is well within the region of well known HMS matrix elements. No HMS optics checks are planned. However, this experiment requires a maximum SOS momentum of 1.74 GeV/c. The $F_\pi - 2$ experiment (E01-004) has successfully performed high quality L/T separations at this momentum, and so are confident that there will be no need for full SOS matrix element fitting. Therefore, we only plan to check the matrix elements by taking a set of sieve-slit data at this (scattered electron) momentum.

Target The use of hydrogen, deuterium and ^{4}He cryogenic targets are proposed for this experiment. Since only two cryo-targets are typically mounted on the ladder at a time, the necessity to switch from ^{1}H to ^{2}H at each beam energy will cause some downtime estimated at 12 hours per change. This downtime has been included as one of the configuration changes in the beam request in Table 5. As the SOS z-target acceptance is limited, we have selected kinematics where the scattered electron angle is no larger than 40°. This allows targets up to 6 cm length to be used. The target windows will be viewed by both spectrometers at most angle settings, so target empty measurements must also be made. We expect the resulting luminosity and rate to be well within the operational experience of previous Hall C standard equipment experiments.

Beam The standard Hall C beamline hardware will be used. In addition to the raster systems, super-harps permit accurate measurements of beam size and angle. The Hall C Moller Polarimeter measures the polarization of the electron beam arriving in Hall C. As shown in the following section, knowledge of the absolute beam polarization is required for the extraction of the polarization-transfer observables. The Hall C Moller operates by observing the rate of production of Moller electrons at $90°$ in the center of mass when the beam strikes a thin iron target. The outer shell electrons in the iron are polarized parallel (or anti-parallel) to the beam direction by a 4 T magnetic field. The Moller electron production rate differs when the beam and target electron spins are aligned parallel or anti-parallel to one-another. Measurement of this rate difference provides a measure of the beam polarization. The Hall C Moller Polarimeter is able to provide an absolute polarization measurement with an accuracy better than 1.5%. Typically, a beam polarization measurement can be carried out in about one hour (plus approximately one hour of setup overhead), and since the electron spin precession from the source to Hall C varies with beam energy, we plan to measure the beam polarization at the beginning of each kinematic setting (typically eight hours of calendar time overhead).

FPP As noted above, the polarization of the recoil proton will be measured in the recently commissioned Focal Plane Polarimeter (FPP) which has been installed in the detector shield house of the HMS in Hall C. Currently, the FPP consists of two (passive) CH_2 analyzer blocks in series, with each one followed by two drift multiwire chambers with a sensitive area of 2.06 m^2; it is shown installed in the HMS detector hut in Fig. 10.

The double polarimeter configuration results in typical efficiencies (*i.e.* the number of incident protons that nuclear scatter in either CH_2 block at a significant polar angle and are detected in the corresponding wire chamber pair) of approximately 40–50%. For this experiment, because of the relatively low proton momentum in the HMS, the thickness of CH_2 in each analyzer will need to be reduced at some kinematic settings. Moreover, installation of the FPP in the HMS detector hut requires the removal of the second layer of triggering scintillators (the so-called "S2" layer). To compensate for this, for the Gep-III/Gep-2γ experiments, a new scintillator detector (known as "S0") was constructed and installed in the space between the exit window of the HMS spectrometer and the HMS wire chambers. At the relatively high proton momenta of these experiments, the multiple scattering is small in S0, and thus HMS tracking is not
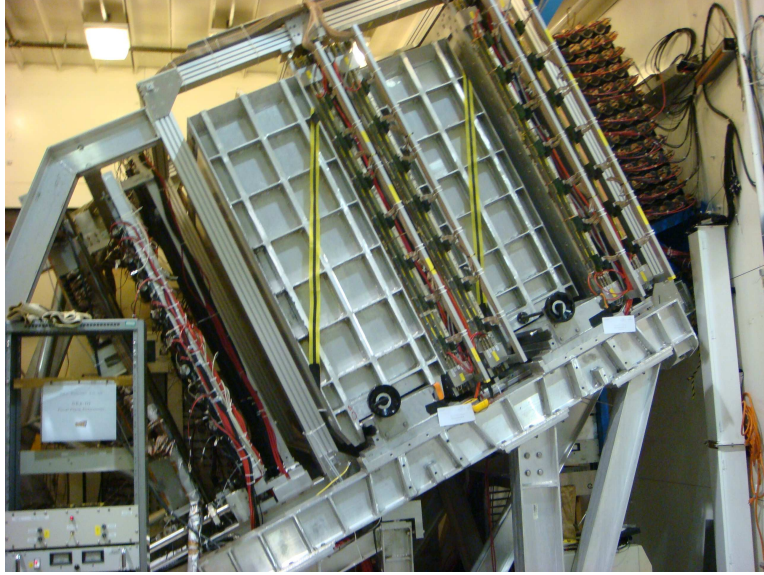
Figure 10: The recently commissioned Focal Plane Polarimeter (FPP) installed in the Hall C HMS detector hut.

significantly affected. However, for the current experiment, this will not be the case. In addition, the S0 detector was constructed to detect primarily elastic protons in scattering from hydrogen, which are confined to a narrow region of the focal plane in the HMS. Therefore, it is simply not large enough to cover the entire focal plane of the HMS, as is required in this proposal.

Thus, we are proposing to construct a new CH_2 analyzer system, which will allow for varying CH_2 thickness, as required for this experiment, and will also serve as an additional trigger layer. For this experiment, we require three thicknesses of analyzer – 5 cm, 20 cm, and 40 cm – to optimize the scattering efficiency in the FPP at the various momentum settings of the HMS. To allow for this optimization, each FPP analyzer will consist of a "passive" CH_2 part, and an "active" scintillator layer, which will provide an additional trigger layer for the experiment, and will also serve as analyzer material. The passive part of each analyzer will consist of "split" CH_2 blocks (to allow for straight-though track calibrations) which will be similar in design to the current system. Each analyzer in the FPP will have two sets of 20 cm-thick blocks. In addition, each analyzer will have an active scintillator layer (behind the passive CH_2 analyzer), consisting of ten (5 cm thick × 15 cm high) horizontal (*i.e.* x-direction) scintillators. Incidentally, we plan to use the existing HMS S2 scintillator readout electronics for the two new scintillator layers. The specific configuration of the analyzers for the range of HMS proton momenta required in this experiment is given shown in Table 2.

The azimuthal distribution of the protons which undergo a second scattering in the analyzer depends upon the proton polarization due to the spin-orbit part of the strong nuclear force [66]. The degree of polarization is directly related to the asymmetry of this angular distribution by:

$$N_p(\theta, \phi) = N_p\Big[1 + (a_i + A_y(\theta)P_y^{fp})\sin\phi + (b_i - A_y(\theta)P_x^{fp})\cos\phi\Big], \qquad (3)$$

where N_p is the number of protons incident on the polarimeter which scatter into a given angular range, and a_i and b_i parameterize instrumental asymmetries. Empirically, the analyzing power, A_y, is the amplitude of the asymmetry resulting from the scattering of a particle with polarization, P_y, i.e. $A_y = \frac{A}{P_y}$. For the proton momenta in this experiment, the analyzing power is well known, from a multitude of experiments at TRIUMF, LAMPF, and in Hall A at JLab.

Table 2: HMS focal plane polarimeter CH_2/scintillator layer configurations for the range of HMS proton momenta in the experiment. FPP1 and FPP2 refer to the first and second analyzers of the polarimeter, respectively.

Proton Momentum	FPP1		FPP2	
Range (GeV/c)	CH_2 (cm)	Scint. (cm)	CH_2 (cm)	Scint. (cm)
$0.500 - 0.700$	-	5.0	-	5.0
$0.700 - 0.900$	20.0	5.0	-	5.0
$0.900 - 1.125$	40.0	5.0	-	5.0
$1.125 - 1.300$	40.0	5.0	20.0	5.0
Above 1.300	40.0	5.0	40.0	5.0

In terms of determining the expected uncertainties in the measured polarization observables, the crucial feature of the polarimeter is its coefficient of merit (COM), defined as COM=$\int_{\vartheta_{min}}^{\vartheta_{max}} \epsilon(\vartheta)A_y^2(\vartheta)d\vartheta \sim \epsilon A_y^2$, where $\epsilon(\vartheta)$ is the differential fraction of events scattered in the analyzer at polar angle ϑ, and $A_y(\vartheta)$ is the corresponding analyzing power. The differential scattering fraction has been estimated from a full Geant3-based simulation of the polarimeter. Estimates obtained for the scattering fraction from this simulation are in good agreement with the results of previous experiments, and are also in agreement with the first commissioning results from the Gep-III/Gep-2γ experiments in Hall C this fall 2007. Thus, we are confident in our estimates for this new experiment.

As the proton travels through the HMS, its spin precesses due to the interaction of the magnetic moment of the proton with the magnetic elements of the HMS, which consists of a series of quadrupole magnets as well as the principal vertical bend dipole magnet.

The proton polarization at the spectrometer focal plane is related to its polarization at the target by a spin matrix:

$$
\begin{pmatrix} \mathbf{P_x^{fp}} \\ \mathbf{P_y^{fp}} \\ P_z^{fp} \end{pmatrix} = \begin{pmatrix} S_{xx} & \mathbf{S_{xy}} & \mathbf{S_{xz}} \\ S_{yx} & \mathbf{S_{yy}} & \mathbf{S_{yz}} \\ S_{zx} & S_{zy} & S_{zz} \end{pmatrix} \begin{pmatrix} P_x^{tar} \\ \mathbf{P_y^{tar}} \\ \mathbf{P_z^{tar}} \end{pmatrix}
$$

The focal plane polarimeter measures only the transverse and normal, P_y^{fp} and P_x^{fp}, components of the proton polarization. The spin matrix is calculated using a model of the spectrometer with the differential-algebra-based transport code COSY. Details are given in Ref. [67] regarding the method for extracting the target polarizations from the knowledge of the spin matrix and measurement of the $N(\theta, \phi)$ distributions. For a standard QQQD magnet spectrometer, the spin matrix components, S_{xx}, S_{yx}, and S_{yz}, are almost zero when averaged over the phase space, and thus for the HMS spectrometer, the systematic uncertainties due to spin precession are expected to be relatively small. In addition, for the purposes of calculating projected uncertainties for this experiment, it is an excellent approximation to consider spin precession in the dipole magnet of the HMS only. In this case, the focal plane polarization components components are written as:

$$P_x^{fp} = P_y^{tar} \cos \chi_{\mathrm{HMS}} \pm h P_z^{tar} \sin \chi_{\mathrm{HMS}} \tag{4}$$

$$P_y^{fp} = \pm h P_x^{tar} \tag{5}$$

where h is the electron beam polarization, and χ_{HMS} is the spin precession angle in the dipole magnet of the HMS. The azimuthal angular distributions of the sum and difference of the two electron beam helicity

states are then, respectively:

$$\frac{N_p^+(\theta, \phi) + N_p^-(\theta, \phi)}{2N_p} = 1 + a_i \sin\phi + (b_i + A_y(\theta)P_y^{tar}\cos\chi_{\mathrm{HMS}})\cos\phi, \tag{6}$$

$$\frac{N_p^+(\theta, \phi) - N_p^-(\theta, \phi)}{2N_p} = hA_y(\theta)P_x^{tar}\sin\phi - hA_y(\theta)P_z^{tar}\sin\chi_{\mathrm{HMS}}\cos\phi. \tag{7}$$

The uncertainty in the Fourier components of these distributions is given by $\sqrt{\frac{2}{N_p}}$, where N_p is the number of protons which scatter in the analyzer in a given angular range. Thus, the uncertainties on the target polarizations are:

$$\sigma(P_x^{tar}) = \sqrt{\frac{2}{N_p h^2 A_y^2}}, \tag{8}$$

$$\sigma(P_y^{tar}) = \sqrt{\frac{2}{N_p A_y^2 \cos^2\chi_{\mathrm{HMS}}}}, \tag{9}$$

$$\sigma(P_z^{tar}) = \sqrt{\frac{2}{N_p h^2 A_y^2 \sin^2\chi_{\mathrm{HMS}}}}. \tag{10}$$

4.2 Rates

Our real rate estimates are based on SIMC [68] Monte Carlo simulations of the Hall C spectrometers, incorporating the actual spectrometer acceptances and radiative effects. We also assume:

- The target length is 6 cm (since the SOS is kept to $\theta < 40^o$ in order to maximize its' y_{target} acceptance).

- The maximum beam current is 100 μA.

- The DAQ rate can be up to 3 kHz for ^{1}H and ^{2}H runs. For ^{4}He, we take a more conservative limit of 2 kHz because of the less favorable online reals/accidentals ratio.

The ^{4}He$(e, e'p)$ real coincidence rate estimates are based on a spectral function model of the form

$$S(p_{recoil}, E_{sep}) = S(p_{recoil})S(E_{sep})$$

where $S(p_{recoil})$ is the Urbana momentum distribution employed by MCEEP [69] for the two-body breakup channel ^{4}He$(e, e'p)^3$H and $S(E_{sep})$ is the ^{4}He$(e, e'p)$ missing energy distribution measured by Richard Florizone, et al. The real coincidence rates listed in Table 4 include no missing mass cuts, while the uncertainties shown in Figs 5, 6, and Table 3 include the effect of spectrometer acceptance and missing mass cuts. The ^{2}H and ^{1}H real coincidence rates are based on parameterizations of existing data, as implemented in SIMC.

Singles rates in the HMS and SOS were examined for $p(e, e'\pi^+)$ data taking [70], and are listed in Table 4. The total singles rates are well below the capability of the detector packages, which were constructed with multi-MHz singles rates in mind. For the purpose of calculating online random coincidence rates, the HMS trigger rate is taken as equal to the raw trigger rate (we do not distinguish pions and protons in the HMS online). Assuming an online π^- rejection rate of 25:1, the SOS trigger rate was taken to be electrons plus $\pi^-/25$. The random coincidence rate is then given by (HMS trigger rate)(SOS trigger rate)Δt, where the coincidence resolving time $\Delta t = 40$ nsec. Where necessary, the beam current used in the rate estimate was adjusted downwards to keep the resulting online real + random rates below 3 kHz for the ^{1}H and ^{2}H runs, and below 2 kHz for the ^{4}He runs. Reliable cross sections have been measured with the Hall C standard equipment and deadtimes $> 50\%$, which corresponds to a rate higher than the upper limit assumed here.

Table 3: Projected uncertainties for the induced polarization and polarization-transfer ratio in the $(\vec{e}, e'\vec{p})$ reaction for ^{1}H elastic data and data on ^{2}H and ^{4}He, integrated over a missing momentum range up to p_m^{max}. The systematic uncertainties for P_y are about 0.005, the systematic uncertainties for P'_x/P'_z are about 0.01; χ_{HMS} is the average spin-precession angle.

| Q^2 | E_{beam} | χ_{HMS} | p_m^{max} | ^{1}H | | ^{2}H, ^{4}He | |
(GeV^2/c^2)	(GeV)	(deg)	(MeV/c)	$\sigma(P_y)$	$\sigma(P'_x/P'_z)$	$\sigma(P_y)$	$\sigma(P'_x/P'_z)$
0.39	1.40	54.8	100	0.0009	0.0072	0.0017	0.0139
0.68	1.85	62.2	100	0.0009	0.0082	0.0016	0.0114
1.38	2.50	80.1	175	0.0043	0.0110	0.0034	0.0139
1.59	2.50	85.2	175	0.0089	0.0142	0.0113	0.0180
2.16	3.00	99.7	175	0.0041	0.0171	0.0054	0.0224
2.42	3.00	106.4	175	0.0034	0.0245	0.0044	0.0321

Offline, the relevant resolving time is 2 nsec and the reals to randoms ratio will be at the few percent level in all cases after further cuts (particle identification and, in the case of the ^{4}He$(e, e'p)$ data, a 5 MeV wide cut around the ^{3}H missing mass).

4.3   Non-physics backgrounds

Once a combination of online hardware and offline software has determined that there was a coincidence between an electron in the SOS and proton in the HMS, there remain several backgrounds of the incoherent 'non-physics' variety: random coincidences and events from the target endcaps.

The electronic coincidence resolving window will be roughly 40 nsec. Offline our excellent coincidence time resolution enables us to reduce the relevant resolving time to 2 nsec with negligible inefficiency. This is the first level of suppression of random coincidences. A 5 MeV wide cut around the ^{3}H missing mass (for the ^{4}He$(e, e'p)$ data) reduces the final random coincidence contamination to the few percent level. The missing (or undetected residual) mass is reconstructed from the final electron and detected hadron 4-momenta:

$$M_{res}^2 = P_{res}^2 = (P_e - P_{e'} + P_{tgt} - P_p)^2$$

A histogram indicating the anticipated missing mass resolution is shown in Fig. 11.

We have chosen the target length to be 6 cm. Because the SOS is kept to a forward angle in this experiment, we expect that both spectrometers will view the end windows in all settings, making window background subtractions a necessity. Because the aluminum windows are each 4 mils thick, the ratio of protons in the windows to protons in the liquid hydrogen is about 10%. However, the surviving window background after cuts is typically found to be only 1%. The reduction from the naive 10% to the measured 1% is presumably due to a combination of final state interactions, SOS y_{target} acceptance, and missing mass cuts. The Hall C "empty" target consists of two 40 mil thick aluminum windows separated by 6 cm, which can tolerate up to 30 μA. Thus, our "empty" data come in 3 times = (40 mil $\times$ 30 μA) /(4 mil $\times$ 100 μA) faster than window events on the real target. We have allocated an amount equal to 10% of the ^{4}He running time for these dummy target runs.

Table 4: Projected SOS and HMS rates from a 6 cm cryogenic target. The HMS+SOS random coincidence rates $(e^- + \pi^-/25) \cdot (\pi^+ + p)$ assume a resolving time of 40 ns and no particle ID or missing mass cuts, thus corresponding to the online rate only; offline cuts will reduce this number to a few percent of the reals. In the case of the hydrogen elastics settings, only the highest rates of that setting are shown.

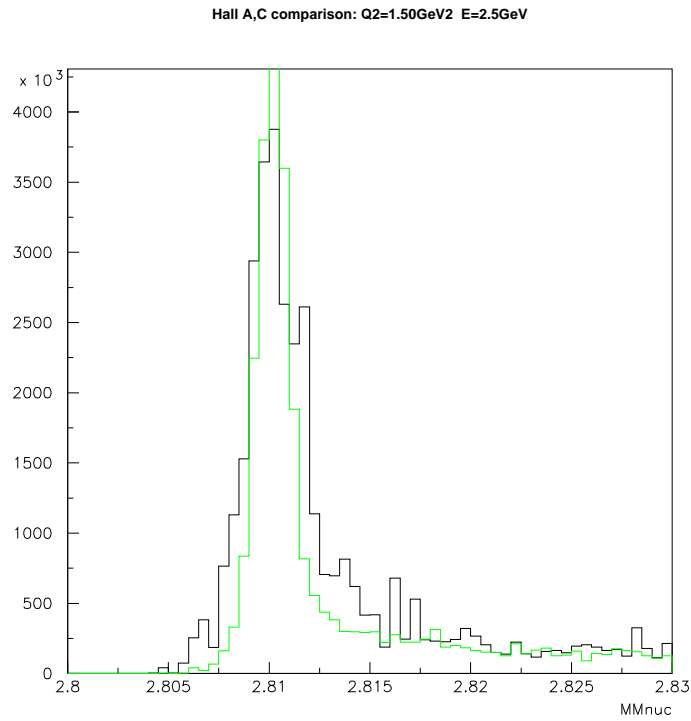| Tgt	p_m (MeV/c)	I (μA)	SOS Singles Rates (kHz)		HMS Singles Rates (kHz)		Random coinc. (Hz)	Real coinc. (Hz)
			e^-	π^-	π^+	p		
Q^2=0.4 (GeV/c)^2, E_e=1.400 GeV								
^{4}He	+0.125	25	121	0	51	247	1440	120
	0.0	35	157	1.0	21	143	1030	565
	-0.125	70	232	38	10	122	1230	499
	-0.225	100	253	181	2.9	109	1160	93
^{2}H	0.0	15	45	0	4.4	15	35	2750
^{1}H	0.0	4.5	11	0	2.5	0.9	1.4	3080
Q^2=0.7 (GeV/c)^2, E_e=1.850 GeV								
^{4}He	+0.250	70	73	0	117	472	1730	30
	+0.125	100	106	0	54	220	1170	349
	0.0	100	115	1.2	16	91	494	853
	-0.125	100	107	28	5.0	62	291	321
	-0.225	100	77	109	1.5	6.8	27	43.2
^{2}H	0.0	40	33	0	3.0	8.9	16	2860
^{1}H	0.0	15	12	0	3.6	2.8	3.0	2670
Q^2=1.5 (GeV/c)^2, E_e=2.500 GeV								
^{4}He	0.0	100	8.7	0.4	0.7	6.1	2.4	153
^{2}H	0.0	100	6.9	0	0.2	20	5.6	836
^{1}H	0.0	100	7.3	0	5.0	9.6	4.3	1425
Q^2=2.3 (GeV/c)^2, E_e=3.000 GeV								
^{4}He	0.0	100	1.7	0.2	0	3.8	0.3	34
^{2}H	0.0	100	1.4	0.1	0	12	0.7	164

Hall A,C comparison: Q2=1.50GeV2 E=2.5GeV

Figure 11: Simulated reconstruction of the ^{3}H missing mass for the $Q^2 = 1.50$ (GeV/c)^2 setting. Black curve: HMS+SOS Green curve: HRS+HRS.

4.4 Beam Request

The beam request allows sufficient events to be acquired to measure the polarization ratios to $\sim 1\%$ at low Q^2, rising to an uncertainty of about 2.5% for the highest Q^2 bin, as listed in Table 3. Projected data for the polarization-transfer superratio as well as for the induced polarization are shown in Fig. 5. Our overhead assumes 8 hours per beam energy change and an additional 12 hour overhead at all except the highest Q^2 for a target configuration change. A summary of the beam request is contained in Table 5.

Table 5: Beam request for hydrogen calibrations, as well as deuterium and helium data taking. The times for each momentum setting are listed in Table 1. These numbers do not include the hall plus equipment data-taking efficiency factor.

Q^2 (GeV^2/c^2)	^{1}H$(\vec{e}, e'\vec{p})$ (Hours)	^{2}H$(\vec{e}, e'\vec{p})n$ (Hours)	^{4}He$(\vec{e}, e'\vec{p})t$ (Hours)	Dummy (Hours)	Overhead (Hours)	Total (Hours)
0.4	6	2	46	5	20	79
0.7	7	2	117	12	20	158
1.5	16	12	83	8	20	139
2.3	0	38	225	22	8	293
Total	29	54	471	47	68	669 (28 days)

4.5 Hall A Option

We prefer to run this experiment in Hall C. However, if Hall C is not available for scheduling or any other reason, then many of the goals of this experiment can be met by the Hall A apparatus. To estimate the beamtime required for the Hall A option, we ran a second set of SIMC [68] simulations making use of the HRS spectrometer optics routines [71] for the "Super Rosenbluth" experiment E01-001 [72]. The kinematics were kept as in Table 1. Since the HRS z-target acceptance is somewhat larger than that of the SOS, the simulations were performed assuming a 10 cm target. The resulting rates and a sample missing momentum versus Q^2 coincidence coverage plot are given in the Appendix.

The smaller solid angles and momentum acceptances of the Hall A standard equipment generally lead to smaller coincidence rates, despite the use of the thicker target. Several of the low Q^2 runs are DAQ rate limited in Hall C, offsetting the effect of the smaller Hall A acceptances, but these are the exception more than the rule. In addition to the lower overall coincidence rate, the larger bend angle of the HRS in comparison to the HMS adversely affects the spin precession of the $Q^2 = 2.30$ (GeV/c)^2 data set, as the 180° spin precession point lies within the acceptance of that setting. If this option is ultimately required, then we would have to consider whether an adjustment to the kinematics is necessary. However, for now we simply considered what additional beamtime would be required to obtain the same statistics. Our simulations indicate that 17 additional days of beamtime would be required to obtain the same statistics if it is not possible to run in Hall C for scheduling or any other reason.

5 Closing Statement

In closing, the question whether nucleon properties are modified by the nuclear medium remains a central issue in nuclear physics. Not only do a wide variety of QCD-based models predict that these changes will occur, but in fact, there is no known way to derive within QCD a nucleus whose constituents do not change properties with increasing density. However, the experimental identification of these modifications is made difficult by the necessary presence of the nuclear medium, which also interacts with the incident and ejectile particles.

The study of the polarization-transfer observables is one of the best ways to reduce the sensitivity to these conventional nuclear medium effects, as they are influenced to a lesser degree by FSI and MEC effects. A further reduction is made by the appropriate choice of target nucleus. ^{4}He is chosen because of its high density but otherwise relative simplicity. Additional control is obtained by measuring the full set of recoil-polarization observables. This is because the induced polarization P_y is dominated by FSI contributions, acting as a control variable, while the polarization transfer ratio (P'_x/P'_z) is used as a probe of any nuclear medium effect.

The existing $^4\mathrm{He}(\vec{e}, e'\vec{p})\,^3\mathrm{H}$ data, including the preliminary results from E03-104, indicate an interesting but unexpected Q^2 dependence which merits further study. In particular, it would be beneficial to greatly improve the precision of the results above $Q^2 > 1.5$ (GeV/c)^2, as different models predict different Q^2 dependences, and so guide whether the assumptions upon which these models are based are warranted. In order to assist in the interpretation of the data, we propose to make comparisons to both ^{1}H and ^{2}H, so that a comparisons can be made both to a free proton, as well as to a bound proton in a low-density nucleus. Finally, it will be helpful to obtain data over a wide range of missing momenta, in order to investigate momentum dependent medium effects. We propose to acquire these data at $Q^2 = 0.4,\ 0.7$ (GeV/c)^2, where the event rates are more favorable. As indicated in Figs. 5 and 6, the proposed data will pose a considerable challenge to medium effect models, including those which allow a role for nucleon structure modifications.

References

[1] S.A. Moszkowski and B.L. Scott, Ann. Phys. **11**, 65 (1960).

[2] R. D. Pisarski, Phys. Lett. **110B**, 155 (1982).

[3] A.W. Thomas, private communication (2003).

[4] G.E. Brown and M. Rho, Phys. Rev. Lett. **66**, 2720 (1991).

[5] R. Rapp, G. Chanfray and J. Wambach, Nucl. Phys. **A617**, 472 (1997).

[6] K. Saito, K. Tsushima and A.W. Thomas, Phys. Rev. C **56**, 566 (1997).

[7] G.Q. Li, Prog. Part. Nucl. Phys. **43**, 619-682 (1999).

[8] G.E. Brown, M. Rho, arXiv: nucl-th/0206021.

[9] X. Jin and D.B. Leinweber, Phys. Rev. C **52**, 3344 (1995).

[10] CERES Collaboration, Th. Ulrich *et al.*, Nucl. Phys. **A610**, 317c (1996).
    G. Agakichiev et al., Phys. Lett. B 422, 405 (1998).

[11] D. Trnka *el al.*, Phys. Rev. Lett. **94**, 192303 (2005).

[12] R. Muto *et al.* Phys. Rev. Lett. **98**, 042501 (2007).

[13] R. Nasseripour *et al.* (CLAS Collaboration), arXiv:0707.2324v4.

[14] K. Saito, K. Tsushima, A.W. Thomas, Prog.Part.Nucl.Phys. **58**, 1-167 (2007).

[15] M. Sargsian *et al.*, J. Phys. G **29**, R1 (2003).

[16] G.A. Miller and J.R. Smith, Phys. Rev. C **65**, 015211 (2001).

[17] G. Miller, private communication (2003).

[18] W. Melnitchouk, K. Tsushima, A.W. Thomas, Eur. Phys. J. A **14**, 105 (2002).

[19] S. Liuti, arXiv:hep-ph/0601125v2.

[20] D.H. Lu, K. Tsushima, A.W. Thomas, A.G. Williams and K. Saito, Phys. Lett. **B417**, 217 (1998) and Phys. Rev. C **60**, 068201 (1999).

[21] J. Jourdan, Phys. Lett. **B353**, 189 (1995).

[22] J. Morgenstern and Z.-E. Meziani, Phys. Lett. **B515**, 269 (2001).

[23] J. Carlson, J. Jourdan, R. Schiavilla, and I. Sick, Phys. Lett. **B553**, 191 (2003).

[24] I. Sick, Comm. Nucl. Part. Phys. **18**, 109 (1988).

[25] T.E.O. Ericson and A. Richter, Phys. Lett. **B183**, 249 (1987).

[26] M.R. Frank, B.K. Jennings and G.A. Miller, Phys. Rev. C **54**, 920 (1996).

[27] U.T. Yakhshiev, U-G. Meissner, and A. Wirzba, arXiv:nucl-th/0211055 (2002).

[28] J.R. Smith and G.A. Miller, Phys. Rev. C **70**, 065205 (2004).

[29] J.W. Van Orden, Phys. Rev. C **74**, 034607 (2006).

[30] H. Arenhövel, private communication (2003).

[31] G. van der Steenhoven *et al.*, Phys. Rev. Lett. **57**, 182 (1986); **58**, 1727 (1987).

[32] P. Ulmer *et al.*, Phys. Rev. Lett. **59**, 2259 (1987).

[33] D. Reffay-Pikeroen *et al.*, Phys. Rev. Lett. **60**, 776 (1988).

[34] T.D. Cohen, J.W. Van Orden, and A. Picklesimer, Phys. Rev. Lett. **59**, 1267 (1987).

[35] A. Magnon *et al.*, Phys. Lett. **B222**, 352 (1989).

[36] J.E. Ducret *et al.*, Nucl. Phys. **A553**, 697c (1993).

[37] J. Carlson *et al.*, Phys. Lett. **B553**, 191 (2003).

[38] A.I. Akhiezer and M.P. Rekalo, Sov. J. Part. Nucl. **3**, 277 (1974); R. Arnold, C. Carlson and F. Gross, Phys. Rev. C **23**, 363 (1981).

[39] M.K. Jones *et al.*, Phys. Rev. Lett. **84**, 1389 (2000).

[40] O. Gayou *et al.*, Phys. Rev. C **64**, 038202 (2001).

[41] O. Gayou *et al.*, Phys. Rev. Lett. **88**, 092301 (2002).

[42] G. Ron *et al.*, Phys. Rev. Lett. **99**, 202002 (2007).

[43] J.M. Laget, Nucl. Phys. A **579**, 333 (1994).

[44] D. Eyl *et al.*, Z. Phys. A **352**, 211 (1995).

[45] B.D. Milbrath, J. McIntyre *et al.*, Phys. Rev. Lett. **80**, 452 (1998).

[46] D.H. Barkhuff, *et al.*, Phys. Lett. B **470**, 39 (1999).

[47] B. Hu *et al.*, Phys. Rev. C **73**, 064004 (2006).

[48] H. Arenhövel, private communication.

[49] D. Gaskell, "Measurement of the EMC Effect in Light Nuclei and at Large x", talk given at the NuINT07 Workshop, May 31, 2007.

[50] S. Dieterich *et al.*, Phys. Lett. **B500**, 47 (2001).

[51] S. Strauch *et al.*, Phys. Rev. Lett. **91**, 052301 (2003).

[52] Jefferson Lab experiment E03-104, *Probing the Limits of the Standard Model of Nuclear Physics with the $^4He(\vec{e}, e'\vec{p})^3H$ Reaction*, R. Ent, R. Ransome, S. Strauch, and P. Ulmer spokespersons.

[53] J. Udias, private communications.

[54] P. Lava *et al.*, Phys. Rev. C **71**, 014605 (2005).

[55] J.M. Udias *et al.*, Phys. Rev. Lett. **83**, 5451 (1991); J.A. Caballero, T.W. Donnelly, E. Moya de Guerra and J.M. Udias, Nucl. Phys. **A632**, 323 (1998); J.M. Udias and J.R. Vignote, Phys. Rev. C **62**, 034302 (2000).

[56] R.J. Woo *et al.*, Phys. Rev. Lett **80**, 456 (1998).

[57] J. Gao *et al.*, Phys. Rev. Lett. **84**, 3265 (2000).

[58] T. de Forest, Nucl. Phys. **A392**, 232 (1983).

[59] J.A. McNeil, L. Ray and S.J. Wallace, Phys. Rev. C **27**, 2123 (1983).

[60] R. Schiavilla *et al.*, Phys. Rev. Lett. **94**, 072303 (2005).

[61] J.J. Kelly, Phys. Rev. C **59**, 3256 (1999).

[62] J.J. Kelly, Phys. Rev. C **60**, 044609 (1999).

[63] T. Horikawa, W. Bentz, Nucl. Phys. A **762**, 102 (2005).

[64] C. Ciofi degli Atti, L.L. Frankfurt, L.P. Kaptari, M.I. Strikman, arXiv:0706.2937v2 [nucl-th].

[65] Jefferson Lab experiment E04-019, *Measurement of the Two-Photon Exchange Contribution in ep Elastic Scattering Using Recoil Polarization*, R. Gilman, L. Pentchev, C. Perdrisat, and R. Suleiman, spokespersons.

[66] E. Aprile-Giboni *et al.*, Nucl. Instrum. Methods **215**, 147 (1983).

[67] V. Punjabi *et al.*, Phys. Rev. C **71**, 055202 (2005), Phys. Rev. C **71**, 069902(E) (2005).

[68] N.C.R. Makins, T.G. O'Neill, and many others, SIMC, Hall C Simulation Package, September 2006 Program Version.

[69] P. Ulmer, MCEEP, Monte Carlo for Electro-Nuclear Coincidence Experiments, Program Version 3.4 (2000).

[70] J. O'Connell and J. Lightbody, Comp. in Phys. May-June **57** (1988) Electron rate: Program QFS, Hadron rates: Program EPC.

[71] J. Arrington, M. Boswell, R. Ent, D. Meekins, and E. Schulte; see `http://hallaweb.jlab.org/data_reduc/AnaWork2001/johna/`

[72] Jefferson Lab experiment E01-001, *New Measurement of G_E/G_M for the Proton*, J. Arrington, R.E. Segel, spokespersons.

A   Projected Rates and Uncertainties for the Hall A Option

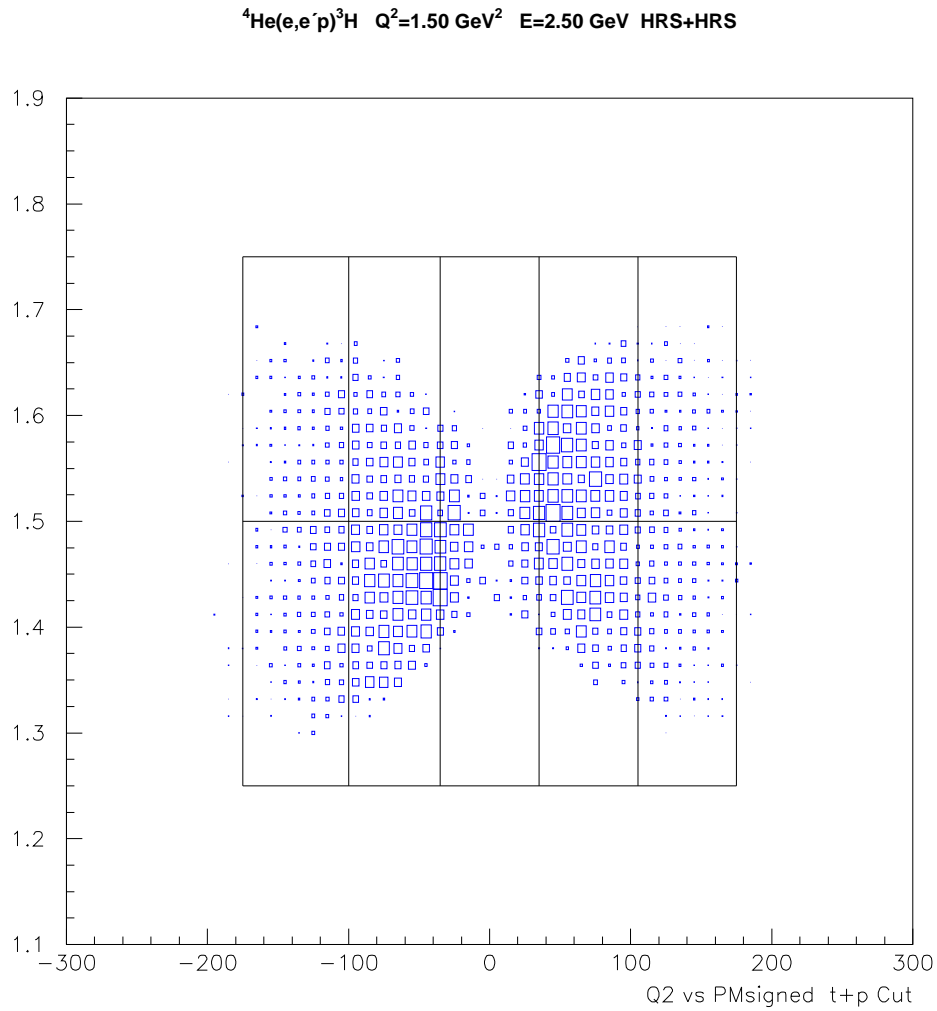Figure 12: Simulated ^{4}He$(e, e'p)^3$H coverage in Q^2 (y-axis) and missing momentum (x-axis) for the $Q^2 = 1.50$ (GeV/c)^2 setting, assuming the HRS+HRS in Hall A. The equivalent coverage using the Hall C equipment is shown in Fig. 7.

Table 6: Projected HRS+HRS rates from a 10 cm cryogenic target. The electron and proton arm random coincidence rates $(e^- + \pi^-/25) \cdot (\pi^+ + p)$ assume a resolving time of 40 ns and no particle ID or missing mass cuts, thus corresponding to the online rate only; offline cuts will reduce this number to a few percent of the reals. In the case of the hydrogen elastics settings, only the highest rates of that setting are shown.

Tgt	p_m (MeV/c)	I (μA)	E-Arm Singles Rates (kHz)		H-Arm Singles Rates (kHz)		Random coinc. (Hz)	Real coinc. (Hz)	Time (Hrs)
			e^-	π^-	π^+	p			
Q^2=0.4 (GeV/c)^2, E_e=1.400 GeV									
^{4}He	+0.125	50	83	0	75	364	1463	101	20
	0.0	70	108	0.7	31	211	1046	634	7
	-0.125	100	106	18	10	120	557	361	8
	-0.225	100	87	62	2.1	80	294	46	27
^{2}H	0.0	25	26	0	5.4	18	24.7	2890	1.5
^{1}H	0.0	4.5	3.6	0	1.9	0.6	0.4	2480	9×0.8
Q^2=0.7 (GeV/c)^2, E_e=1.850 GeV									
^{4}He	+0.250	100	36	0	123	497	893	6.8	230
	+0.125	100	37	0	40	162	296	145	26
	0.0	100	40	0.4	12	67	125	501	9
	-0.125	100	37	9.6	3.7	46	74	183	18
	-0.225	100	27	38	1.1	5.1	6.8	24	51
^{2}H	0.0	60	17	0	3.3	9.8	8.8	2980	1.5
^{1}H	0.0	15	4.0	0	2.7	2.1	0.8	2420	9×1.0
Q^2=1.5 (GeV/c)^2, E_e=2.500 GeV									
^{4}He	0.0	100	3.0	0.1	0.4	4.5	0.6	103	120
^{2}H	0.0	100	2.4	0	0.2	15	1.4	737	13
^{1}H	0.0	100	2.5	0	3.7	7.1	1.1	1690	9×1.6
Q^2=2.3 (GeV/c)^2, E_e=3.000 GeV									
^{4}He	0.0	100	0.6	0.06	0	2.8	0.07	27	330
^{2}H	0.0	100	0.5	0.05	0	9.1	0.17	171	38

Table 7: Projected uncertainties for the induced polarization and polarization-transfer ratio in the $(\vec{e}, e'\vec{p})$ reaction for ^{1}H elastic data and data on ^{2}H and ^{4}He (Hall A Option), integrated over a missing momentum range up to p_m^{max}. The systematic uncertainties for P_y are about 0.015, the systematic uncertainties for P_x'/P_z' are about 0.01; χ_{HRS} is the average spin-precession angle.

Q^2 (GeV^2/c^2)	E_{beam} (GeV)	χ_{HMS} (deg)	p_m^{max} (MeV/c)	^{1}H $\sigma(P_y)$	^{1}H $\sigma(P_x'/P_z')$	^{2}H, ^{4}He $\sigma(P_y)$	^{2}H, ^{4}He $\sigma(P_x'/P_z')$
0.39	1.40	98.6	100	0.0034	0.0064	0.0066	0.0124
0.68	1.85	111.9	100	0.0011	0.0064	0.0020	0.0113
1.44	2.50	146.5	175	0.0007	0.0128	0.0009	0.0163
1.56	2.50	152.1	175	0.0009	0.0175	0.0011	0.0222
2.21	3.00	186	175	0.0007	0.0306	0.0009	0.0400
2.38	3.00	189.7	175	0.0010	0.0459	0.0013	0.0600

Table 8: Beam request for the Hall A option, to be used only in the case that Hall C is unavailable for scheduling or other reasons. The times for each momentum setting are listed in Table 6.

Q^2 (GeV^2/c^2)	^{1}H($\vec{e}, e'\vec{p}$) (Hours)	^{2}H($\vec{e}, e'\vec{p}$)n (Hours)	^{4}He($\vec{e}, e'\vec{p}$)t (Hours)	Dummy (Hours)	Overhead (Hours)	Total (Hours)
0.4	8	2	62	6	20	98
0.7	9	2	334	34	20	399
1.5	15	13	120	12	20	180
2.3	0	38	330	33	8	409
Total	32	55	846	85	68	1086 (45 days)